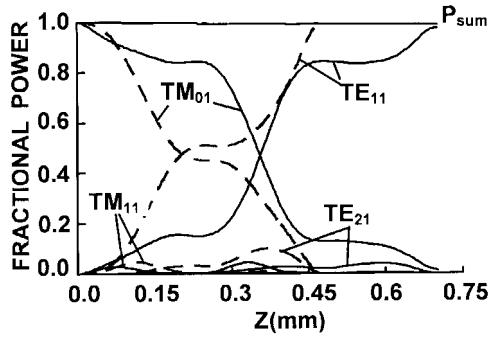

Fig. 4. Calculated fractional power distributions for the TM_{01}–TE_{11} mode converter of Case (a) (solid line) and Case (c) (dashed line) in Table II.

TABLE II
OPTIMIZED CHARACTERISTIC RESULTS FOR TM_{01}–TE_{11} MODE CONVERTERS FORMED BY NONCONSTANTLY BENT WAVEGUIDES ($f_0 = 35$ GHz, $a_0 = 13.6$ mm)

Case	Sinusoidal (a)	Cub. Parabo. (b)	Gaussian (c)
Axis coordinate:	Eq. (6)	Eq. (7)	Eq. (8)
Geometrical characteristics:	ε_1=0.0162m W_1=0.6971m ε_2=0.0002m W_2=0.1800m ε_3=0.0007m W_3=0.2781m	ε_1=1.5810m^{-2} ε_2=-0.0001m W_2=0.1595m ε_3=0.0011m W_3=0.2796m	ε_1=0.1000m δ=14.085m^{-2} ε_2=-0.0004m W_2=0.2067m ε_3=-0.0015m W_3=0.2798m
Total converter length:	0.7008m	0.4749m	0.4715m
Output power levels: TM_{01}	0.0125	0.0010	0.0002
TE_{11}	0.9756(η)	0.9857(η)	0.9887(η)
TM_{11}	0.0001	0.0025	0.0004
TE_{21}	0.0005	0.0016	0.0003
TE_{01}	0.0012	0.0027	0.0040
Power transmission efficiency: P_{sum}	0.9900	0.9935	0.9936
Bandwidth factor ($\eta \geq 90\%$): $\Delta f/f_0$	21.1%	28.2%	27.1%

cubic parabola mode converter has an antisymmetry about its center ($x = 0$), and the Gaussian mode converter takes a segment of the Gaussian curve's left side ($x < 0$). The two additional, continuous phase-rematching small perturbations ε_2 and ε_3 are used to suppress the TM_{11} and TE_{21}, respectively. All the calculated results of the three TM_{01}–TE_{11} mode converters for $f_0 = 35$ GHz and $a_0 = 13.6$ mm, corresponding to Cases (a), (b), and (c) are summarized in Table II. Fig. 4 demonstrates the normalized power distributions for Cases (a) and (c) in Table II. The distributions for Case (b) are similar to that of Case (c) and are not plotted in Fig. 4.

IV. CONCLUSION

Direct short TM_{01}–TE_{11} mode converters with high conversion efficiencies and large bandwidth factors may be realized by bent waveguides with elaborately chosen shapes and optimized geometrical dimensions. Five examples of TM_{01}–TE_{11} mode converters with different structures for $f_0 = 35$ GHz and waveguide radius $a_0 = 27.2$ mm are presented, with each one having its own features. All of the five mode converters can have high conversion efficiencies of $\eta > 97.5\%$ and large bandwidth factors (for $\eta \geq 90\%$) of greater than 21%.

REFERENCES

[1] M. Thumm, A. Jacobs, and M. S. Ayza, "Design of short high-power TM_{01}–TE_{11} mode converters in highly overmoded corrugated waveguides," *IEEE Trans. Microwave Theory Tech.*, vol. 39, pp. 301–309, Feb. 1991.
[2] M. Thumm, "High-power millimeter wave mode converters in overmoded circular waveguides using periodic wall perturbations," *Int. J. Electron.*, vol. 57, pp. 1225–1246, Dec. 1984.
[3] M. Thumm, "High power mode conversion for linearly polarized HE_{11} hybrid mode output," *Int. J. Electron.*, vol. 61, pp. 1135–1153, Dec. 1986.
[4] J. L. Doane, "Mode converters for generating the HE_{11} (Gaussian-like) mode from TE_{01} in a circular waveguide," *Int. J. Electron.*, vol. 53, pp. 573–585, Dec. 1982.
[5] S. W. Yang and H. F. Li, "A study on TM_{0n}–TM_{01} mode converters of circular waveguides," *Chinese J. Univ. of Elec. Sci. and Tech. of China*, vol. 22, supp., pp. 118–124, Dec. 1993.
[6] ——, "Numerical modeling of 8 mm TM_{01}–TE_{11} mode converter," *Int. J. Infrared Millim. Waves*, vol. 16, pp. 1935–1943, Nov. 1995.
[7] H. F. Li and M. Thumm, "Mode conversion due to curvature in corrugated waveguides," *Int. J. Electron.*, vol. 71, pp. 333–347, Aug. 1991.

Characteristic Impedance of a Rectangular Double-Ridged TEM Line

Khona Garb and Raphael Kastner

***Abstract*— The characteristic impedance of a TEM transmission line, shaped as a double-ridged rectangular coaxial line, is analyzed in this paper as the customary transversal static problem. This type of transmission line is useful, for example, as a part of a cascaded transition between a double-ridged waveguide and a coaxial line. The solution of the transversal problem is achieved by dividing the cross-sectional region into distinct, separable regions, each one being characterized by a closed-form Green's functions relating the flux function to the electric field. Surface-type integral equations are then formulated over the boundaries between the regions. Solution of these equations via the method of moments (MoM's) using the Galerkin choice yields the results for the characteristic impedance as a function of cross-sectional dimensions. Convergence of the solution is also studied.**

***Index Terms*— Characteristic impedance, Galerkin method, ridged TEM line.**

I. INTRODUCTION

Transmission lines operating in the TEM regime are widely used in microwaves circuits. In many cases, TEM and non-TEM devices need to be connected in a cascaded configuration, requiring a transition between the two types of lines. Such a transition would possess some of the geometrical features of the two lines at both ends. In the case treated in this paper, a transition between a coaxial TEM line and a double-ridged waveguide has been devised. Several rectangular

Manuscript received October 29, 1996; revised December 24, 1996.
The authors are with the Department of Electrical Engineering–Physical Electronics, Tel Aviv University, Tel Aviv 69978, Israel.
Publisher Item Identifier S 0018-9480(97)02541-6.

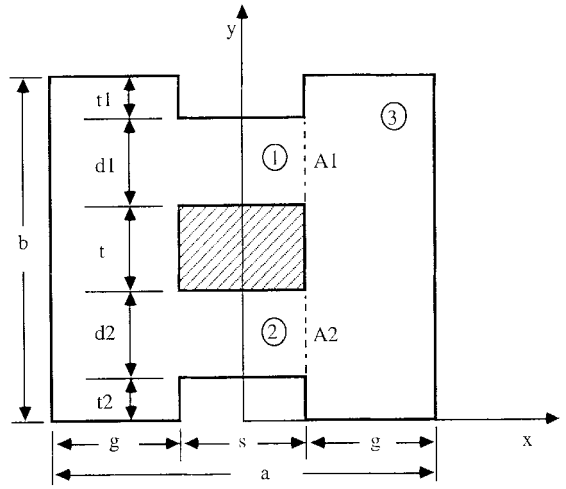

Fig. 1. Cross section of a rectangular ridged TEM line.

TEM configurations have been reported in the literature [1]–[3]. The configuration chosen in this paper is a double-ridged coaxial transmission line with rectangular cross section as seen in Fig. 1. In the absence of the ridges $(t_1 = t_2 = 0)$, the transmission line of Fig. 1 becomes a rectangular coaxial line. For this line, the characteristic impedance Z_0 for the case of a symmetric position of the inner conductor $(d_1 = d_2)$ has been evaluated in the literature by a number of methods [4]–[6]. In [4], the conformal mapping technique has been used to derive closed-form expressions for Z_0. The relaxation process was utilized in [5] to solve finite-difference equations, resulting in a comprehensive set of graphs of Z_0 as a function of the cross-sectional dimensions. An improved approximation for Z_0 is given in [6] for the symmetrical rectangular coaxial line. A summary of data for calculating Z_0 for many rectangular TEM configurations can be found in [2].

The examples cited above do not include the case of the ridged TEM line, which apparently has not received attention in the literature to date. Out of several methods eligible for the solution of this problem, the authors have chosen the surface integral equation approach. This approach takes advantage of the fact that the cross section can be divided into a finite number of separable regions, such that the problem can be defined over the interfaces between adjacent regions. The computational domain is thus limited to a set of straight lines rather than to the cross-sectional plane in its entirety. Within each one of these regions, the known analytical Green's function is used to generate a surface description of the region, relating the tangential electric field and the flux function. The different regions are joined together by invoking the requirement that the flux function and its normal derivative be continuous across the interfaces. More specifically, the problem is defined over the lines denoted A_1 and A_2, forming the interfaces between regions 1 and 3 and between 2 and 3, respectively (see Fig. 1). The remaining (conducting) boundaries are already included in the formulation of the Green's functions. The boundary condition leads to a set of integral equations for the tangential electric field $E_i(y)$ on $A_i, (i = 1, 2)$. This system of integral equations is discretized using the Galerkin version of the method of moments (MoM's) with entire domain cosinusoidal basis and testing functions. The solution of the integral equation is then used for the evaluation of the capacitance per-unit length and the characteristic impedance Z_0, both expressed as functionals of $E_i(y)$. The convergence of the method is discussed, and it is shown that the values of Z_0 tend to increase with an increasing number of basis functions. It is thus concluded that the true value of Z_0 is an upper bound value for the numerical calculations.

II. Integral Equation Formulation

The cross-sectional structure of the ridged TEM line (Fig. 1) exhibits symmetry around the plane $x = 0$, allowing for the problem to be defined over the region $x > 0$ only. Using the Green's theorem, which relates $E_i(y)$ to the flux function, and the continuity of the flux function and its normal derivative across the boundaries on A_i, $(i = 1, 2)$, one can formulate the following system of integral equations in the y-directed component of the electric field $E_i(y)$ on the interfaces

$$\int_{A_1} dy_1'[G_1(y_1, y_1') + G_3(y_1, y_1')]E_1(y_1') + \int_{A_2} dy_2' G_3(y_1, y_2')E_2(y_2') = B_1 \tag{1}$$

$$\int_{A_1} dy_1' G_3(y_2, y_1')E_1(y_1') + \int_{A_2} dy_2'[G_2(y_2, y_2') + G_3(y_2, y_2')]E_2(y_2') = B_2 \tag{2}$$

where

$$G_i(y_i, y_i') = \frac{1}{2}\left[\frac{s}{d_i} + \frac{4}{\pi}\sum_{n=1}^{\infty}\frac{1}{n}\cos\left(\frac{n\pi\overline{y_i}}{d_i}\right)\cos\left(\frac{n\pi\overline{y_i}'}{d_i}\right)\tanh\left(\frac{n\pi s}{2d_i}\right)\right], \quad i = 1, 2 \tag{3}$$

with

$$\overline{y_1} = y_1 - (t_2 + d_2 + t)\ and\ \overline{y_2} = y_2 - t_2 \tag{4}$$

(see Fig. 1), and

$$G_3(y_i, y_j') = \frac{2}{\pi}\sum_{n=1}^{\infty}\frac{1}{n}\cos\left(\frac{n\pi y_i}{b}\right)\cos\left(\frac{n\pi y_j'}{b}\right)\coth\left(\frac{n\pi g}{b}\right), \quad i, j = 1, 2 \tag{5}$$

such that G_i is the Green's function for region $\#i$, and y_i is defined over interface A_i. These functions are constructed in accordance with the Dirichlet boundary condition along $x = 0$ for regions 1 and 2, and the Neumann condition over all other surfaces for each region. The unknowns B_i in the system of (1), (2) are constants, stemming from the fact that the balance between the flux values on both sides of the interfaces can only be determined up to a constant. These constants are dependent upon the excitation (i.e., they are proportional to the potential difference U between the outer and inner conductors). U is defined as follows:

$$U = \int_{A_1} dy_1 E_1(y_1) = -\int_{A_2} dy_2 E_2(y_2). \tag{6}$$

Equations (1) and (2) are thus used jointly with the constraint (6). U can be chosen arbitrarily, resulting in proportional values for B_1 and B_2. A convenient choice would be $U = 1$.

The capacitance per-unit length C via energy calculations is now evaluated. The electrical energy stored in the transmission line per-unit length can be expressed as the following surface integral over the cross section:

$$\begin{aligned} W =& \frac{1}{2}\epsilon\int |\mathbf{E}|^2 dS \\ =& \epsilon\Bigg\{\int_{A_1} dy_1 \int_{A_1} dy_1' E_1(y_1)[G_1(y_1, y_1') + G_3(y_1, y_1')]E_1(y_1') \\ &+ 2\int_{A_1} dy_1 \int_{A_2} dy_2' E_1(y_1) G_3(y_1, y_2')E_2(y_2') \\ &+ \int_{A_2} dy_2 \int_{A_2} dy_2' E_2(y_2)[G_2(y_2, y_2') + G_3(y_2, y_2')]E_2(y_2')\Bigg\} \end{aligned} \tag{7}$$

TABLE I
CONVERGENCE OF THE CHARACTERISTIC IMPEDANCE OF A SQUARE COAXIAL LINE USING THE GALERKIN PROCEDURE

$N_1 = N_2$	$\frac{s}{a} = .1$	$\frac{s}{a} = .3$	$\frac{s}{a} = .5$	$\frac{s}{a} = .7$	$\frac{s}{a} = .9$
1	113.05	63.51	35.84	17.79	5.056
2	126.57	65.90	36.52	17.95	5.069
3	129.52	66.37	36.66	17.99	5.072
4	130.65	66.55	36.71	18.00	5.073
5	131.21	66.64	36.74	18.01	5.074
6	131.55	66.69	36.76	18.01	5.075
7	131.77	66.73	36.77	18.01	5.075
8	131.92	66.76	36.77	18.02	5.075
9	132.04	66.78	36.78	18.02	5.075
10	132.12	66.79	36.78	18.02	5.075
11	132.19	66.80	36.79	18.02	5.075
12	132.25	66.81	36.79	18.02	5.075
13	132.29	66.82	36.79	18.02	5.075
15	132.36	66.83	36.80	18.02	5.075
16	132.39	66.83	36.80	18.02	5.075
17	132.41	66.84	36.80	18.02	5.075
18	132.43	66.84	36.80	18.02	5.075
19	132.45	66.84	36.80	18.02	5.075
20	132.47	66.85	36.80	18.02	5.075
[2]	132.65	66.87	36.81	18.02	—

where ϵ is the dielectric permittivity of the medium between the conductors. Equation (7) can also be interpreted, in view of (1), (2) as follows:

$$W = \epsilon\left[B_1 \int_{A_1} dy_1 E_1(y_1) + B_2 \int_{A_2} dy_2 E_2(y_2)\right]. \tag{8}$$

The capacitance C then becomes

$$C = \frac{2W}{U^2} = 2\epsilon\left[\frac{B_1}{\int_{A_1} dy_1 E_1(y_1)} + \frac{B_2}{\int_{A_2} dy_2 E_2(y_2)}\right] \tag{9}$$

using the definitions (6) for U. Choosing $U = 1$ and computing B_1 and B_1 accordingly, one obtains

$$C = 2\epsilon[B_1 - B_2]\, F/m. \tag{10}$$

The characteristic impedance of the line may now be found for C via

$$Z_0 = \frac{1}{\sqrt{\epsilon_r}}\zeta_0 \frac{1}{C/\epsilon}. \tag{11}$$

Here, ϵ_r is the relative permittivity of the medium, and $\zeta_0 = 376.678\Omega$ is the free-space wave impedance.

III. NUMERICAL SOLUTION OF THE PROBLEM

The system of (1), (2) is solved by the MoM's, where $E_i(y)$ is expanded by a series of cosinusoidal basis functions, as follows:

$$E_i(y_i) = \sum_{\nu=1}^{N_i} D_\nu^{(i)} \chi_\nu^{(i)}(\overline{y_i})$$

$$\chi_\nu^{(i)}(\overline{y_i}) = \frac{1}{d_i}\cos\left[\frac{(\nu-1)\pi\overline{y_i}}{d_i}\right], \qquad \nu = 1, 2, \cdots, N_i \tag{12}$$

and $\overline{y_{1,2}}$ are defined in (4). Testing (1), (2) by the Galerkin scheme, one obtains the system of linear algebraic equations of the order $N = N_1 + N_2 + 2$. Solution of this system yields the coefficients $D_\nu^{(i)}$ as well as B_i.

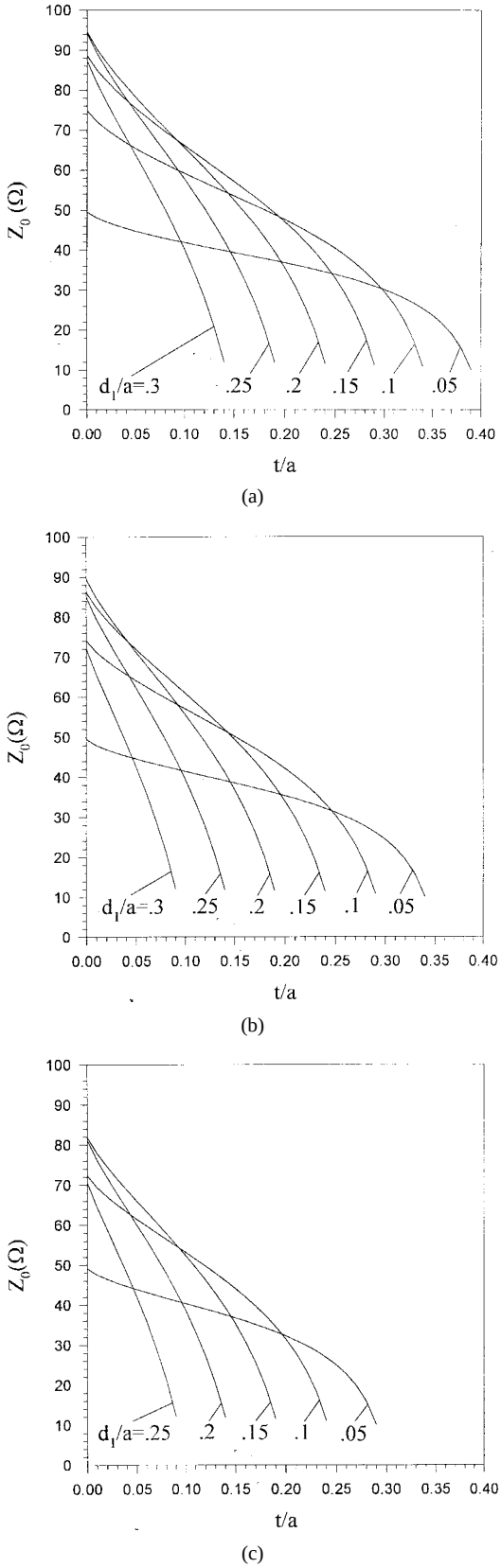

Fig. 2. Characteristic impedance of a rectangular ridged TEM line versus inner conductor height t; $b/a = 0.5$, $s/a = 0.25$, $t_2/a = 0$. (a): $t_1 = 0.05$. (b): $t_1 = 0.10$.(c): $t_1 = 0.15$.

The results computed in this way are presented in Table I. They illustrate the stable convergence characteristics of the impedance Z_0

of the square coaxial line ($a = b, s = t, t_1 = t_2 = 0$) as the number of basis functions $N_1 = N_2$ is increased. In the last line of Table I the exact values for the square coaxial line are listed as quoted from [2]. One may observe that the values of Z_0 tend to increase with an increasing number of basis functions, such that as $N_1 \to \infty$ the value of Z_0 as computed here increases monotonically toward the exact value.

For the case of the rectangular coaxial line, computed with $N_1 = N_2 = 20$, the authors' results coincide with those from [5]. Fig. 2 shows the characteristic impedance as a function of the height of the inner conductor t, with various other parameters. These figures can be used for design purposes when transitions between ridged waveguides and coaxial lines are needed.

REFERENCES

[1] J. C. Dix, "Design of waveguide/coaxial transition for the band 2.5-4.1 Gc/s," *Proc. Inst. Elect. Eng.*, vol. 110, no. 2, pt. H, pp. 253-255, Feb. 1963.

[2] M. A. R. Gunston, *Microwave Transmission Line Impedance Data*. New York: Van Nostrand, 1972

[3] E. A. Navarro, V. Such, B. Gimeno, and J. L. Cruz, "T-junctions in square coaxial waveguide: An FD-TD approach," *IEEE Trans. Microwave Theory Tech.*, vol. 42, pp. 347-350, Feb. 1994.

[4] A. Matsumoto, Ed., *Microwave Filters and Circuits. Supplement 1 to Advances in Microwaves*. New York: Academic Press, 1970, ch. 5.

[5] W. S. Metcalf, "Characteristic impedance of rectangular transmission lines," *Proc. Inst. Elect. Eng.*, vol. 112, no. 11, pt. H, pp. 2033-2039, Nov. 1965.

[6] H. J. Riblet, "Upper limits on the error of an improved approximation for the characteristic impedance of rectangular coaxial line," *IEEE Trans. Microwave Theory Tech.*, vol. MTT-28, pp. 666-667, June 1980.

Propagation Characteristics of a Dielectric-Coated Coaxial Helical Waveguide in a Lossy Medium

Takahiro Iyama and Jun-ichi Takada

***Abstract*—In this paper, the authors discuss the propagation characteristics of a dielectric-coated coaxial helical waveguide in a lossy medium. The authors place emphases on the phase constant, propagation modes, magnetic fields distribution, and attenuation constant. When permittivity of the internal region is relatively small, two propagation modes exist and dominant components of their magnetic fields are different. Lastly, the authors discuss the relation between the attenuation constant and permittivities.**

***Index Terms*—Absorbing media, helical waveguide, hyperthermia.**

I. INTRODUCTION

Coaxial helical waveguides have been studied by Hill and Wait [1], Wait [2], Mirotznik *et al.* [3], and other researchers. In those papers, the bared or noncoated helices were discussed. In this paper, the authors discuss the theoretical propagation characteristics of a dielectric-coated coaxial helical waveguide in a lossy medium. This structure corresponds to the coaxial helical applicator for microwave hyperthermia which is covered with a catheter.

Manuscript received November 22, 1996; revised December 24, 1996

The authors are with the International Cooperation Center for Science and Technology, Tokyo Institute of Technology, Meguro-ku, Tokyo 152 Japan.

Publisher Item Identifier S 0018-9480(97)02536-2.

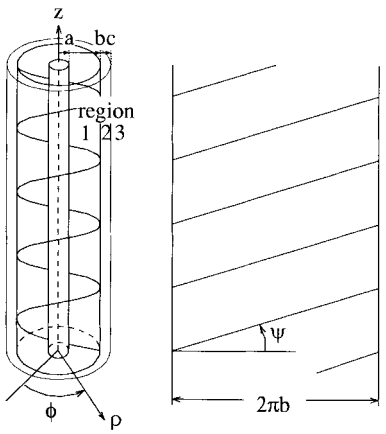

Fig. 1. Perspective view of a dielectric-coated coaxial helical waveguide constructed of three layers.

II. FORMULATION

The analysis model is shown in Fig. 1. The inner conductor of radius a is perfectly conducting, and the helical wire is wound at $\rho = b$ with pitch angle ψ. The model is divided into three regions as:

$$a < \rho < b: \text{region } 1 \text{ (permittivity } \varepsilon_1)$$
$$b < \rho < c: \text{region } 2 \text{ (permittivity } \varepsilon_2)$$
$$c < \rho: \text{region } 3 \text{ (permittivity } \varepsilon_3).$$

The permeability μ_0 is constant for all regions. The authors assume that the variations of the electric and magnetic fields in the z-direction is $\exp(-\gamma \cdot z)$ and those in the ϕ-direction is constant; γ is the complex propagation constant along the z-direction. At $\rho = b$, the boundary conditions are represented by the sheath helix model, i.e., the cylindrical surface at $\rho = b$ is assumed to have anisotropic conductivity that the surface current can flow along only the ψ-direction. With those assumptions, the authors obtain the following Maxwell's equations in the cylindrical coordinates:

$$\frac{\partial^2 H_z}{\partial \rho^2} + \frac{1}{\rho}\frac{\partial H_z}{\partial \rho} + (\omega^2 \varepsilon \mu_0 + \gamma^2) H_z = 0 \tag{1}$$

$$E_\phi = \frac{j\omega\mu_0}{\omega^2 \varepsilon \mu + \gamma^2}\frac{\partial H_z}{\partial \rho} \tag{2}$$

$$\frac{\partial^2 E_z}{\partial \rho^2} + \frac{1}{\rho}\frac{\partial E_z}{\partial \rho} + (\omega^2 \varepsilon \mu_0 + \gamma^2) E_z = 0 \tag{3}$$

$$H_\phi = -\frac{j\omega\varepsilon}{\omega^2 \varepsilon \mu_0 + \gamma^2}\frac{\partial E_z}{\partial \rho} \tag{4}$$

where ω is the angular frequency. The appropriate solutions in region 1 and 2 are

$$H_z = A_i I_0(\kappa_i \rho) + B_i K_0(\kappa_i \rho) \tag{5}$$

$$E_\phi = -\frac{j\omega\mu}{{\kappa_i}^2}[A_i I_0'(\kappa_i \rho) + B_i K_0'(\kappa_i \rho)] \tag{6}$$

$$E_z = A_i^* I_0(\kappa_i \rho) + B_i^* K_0(\kappa_i \rho) \tag{7}$$

$$H_\phi = \frac{j\omega\varepsilon_i}{{\kappa_i}^2}[A_i^* I_0'(\kappa_i \rho) + B_i^* K_0'(\kappa_i \rho)], \qquad i = 1, 2 \tag{8}$$